

Kondo spectral functions at low-temperatures: A dynamical-exchange-correlation-field perspective.

Zhen Zhao^{1*}

1 Division of Mathematical Physics and ETSE, Lund University, PO Box 118, 221 00 Lund,
Sweden

* zhen.zhao@teorfys.lu.se

Abstract

We calculate the low-temperature spectral function of the symmetric single impurity Anderson model using a recently proposed dynamical exchange-correlation (xc) field formalism. The xc field, coupled to the one-particle Green's function, is obtained through analytic analysis and numerical extrapolation based on finite clusters. In the Kondo regime, the xc field consists of a complex constant term and a main quasiparticle-like oscillation term. The constant term represents the Hubbard side-band contribution, containing a bath-induced broadening effect, while the quasiparticle-like term is related to the Kondo resonance peak at low-temperature. We illustrate these features in terms of analytical and numerical calculations for small and medium-size finite clusters, and in the thermodynamic limit. The results indicate that the xc field formalism provides a good trade-off between accuracy and complexity in solving impurity problems. Consequently, it can significantly reduce the complexity of the many-body problem faced by first-principles approaches to strongly correlated materials.

Copyright attribution to authors.

This work is a submission to SciPost Physics.

License information to appear upon publication.

Publication information to appear upon publication.

Received Date

Accepted Date

Published Date

1

2 Contents

3	1 Introduction	2
4	2 Theory	3
5	2.1 V _{xc} formalism for the SIAM	4
6	2.2 The SIAM V _{xc} at low-temperature	6
7	3 Results	7
8	3.1 Analytic insights from a dimer	7
9	3.2 Including hybridization with a finite cluster at zero- <i>T</i>	8
10	3.3 Ansatz of the symmetric SIAM V _{xc}	9
11	4 Conclusions and outlook	12
12	A Low temperature approximation of the V_{xc}	13
13	B Analytic V_{xc} of an impurity-free-electron dimer	14

14	C Solving the Green's function from the ansatz of the Vxc	16
15	References	16

16
17

18 1 Introduction

19 Quantum impurity models (QIMs), where one impurity (with a small number of discrete lev-
20 els) is coupled to a noninteracting bath (with continuous degrees of freedom), have been
21 extensively studied during the past decades. Originally proposed to study the Kondo ef-
22 fect [1] (where a localized spin is screened by conducting electrons due to many-body cor-
23 relations), QIMs remain to this date the focus of vast interest for their applicability to different
24 topical areas, such as quantum transport through nanoscale devices [2–4], tunneling spec-
25 troscopy [5–7], and many-body entanglement [8, 9]. Moreover, the single-impurity Anderson
26 model (SIAM) [10], one of the basic QIMs variants, is used as an auxiliary problem for dy-
27 namical mean-field theory (DMFT) [11], a tool in first-principles studies of strongly correlated
28 systems in- and out-of-equilibrium [12–14].

29 Because of this important usage, several types of quantum impurity solvers for the SIAM
30 have been developed. The thermodynamic properties of the SIAM can be exactly solved by
31 the numerical renormalization group (NRG) [15], the continuous-time quantum Monte Carlo
32 (QMC) algorithm [16] and Bethe-ansatz based analytic approaches [17–19]. However, the
33 direct application of these solvers to the spectral properties of the SIAM is restricted by factors
34 such as the high computational cost of the original NRG, and the dynamical sign problem or
35 artifacts introduced by the analytic continuation in QMC. Hence advanced solvers arise with
36 sophisticated numerical methods, including generalized NRG [20–23], functional renormal-
37 ization group [24, 25], configuration interaction approximations [26], distributional exact di-
38 agonalization (ED) [27, 28], steady state density functional theory (DFT) [29–31], expansion
39 QMC [32–34], and non-wave-function-based tensor network approaches [35, 36].

40 Nonetheless, in spite of these significant advances, there remains a demand for a theoretical
41 treatment of the SIAM which can i) capture spectral weights and energy scales of the Kondo
42 peak and the Hubbard bands in a conceptually and physically transparent way, and ii) be
43 computationally inexpensive (in order to make significantly numerically affordable those *ab*
44 *initio* treatments that use SIAM as an auxiliary problem).

45 Recently, a Green's function-based dynamical exchange-correlation (xc) field formalism
46 [37] was proposed. Given the key quantity in the framework, the dynamical xc field (Vxc),
47 the single-particle Green's function (and thus the spectral function) can be solved by a direct in-
48 tegral in the time domain. The Vxc has been calculated exactly for one-dimensional (1D) finite
49 lattice models [38, 39] and within the random-phase approximation for the homogeneous elec-
50 tron gas [40]. For those systems, the temporal behavior of the Vxc, $V^{xc}(t) \sim V_0 + \sum_n A_n e^{-i\omega_n t}$,
51 can be seen as the sum of a constant term (complex for the homogeneous electron gas) plus
52 a small number of oscillating terms accounting for quasiparticle-like excitations. Accordingly,
53 the spectral weight is mainly distributed among a sharp peak (from the constant term V_0)
54 and continuous satellite bands that emerge from the oscillating terms in Vxc. Thus, a central
55 task in the approach is to determine the parameters defining Vxc, which naturally implies the
56 introduction of approximate estimates. For example, when applied to 1D half-filled Hubbard
57 lattice and spin- $\frac{1}{2}$ antiferromagnetic Heisenberg lattice at zero temperature, the formalism
58 approximates the exact lattice Vxc using finite clusters [38, 39]. Consequently, the spectral

59 functions are calculated with a good trade-off between accuracy and computational cost. The
 60 quasiparticle-like excitations in the Vxc and the favourable spectral results may be explained
 61 by a dynamical screening effect: at zero-temperature, exchange potential and many-body cor-
 62 relations together suppress many degrees of freedom and lead to only few (if not only one)
 63 dominant excitations ω_n .

64 In the local moment regime, some central features of the SIAM local spectral function have
 65 an immediate interpretation in terms of the Vxc language. Namely, the Hubbard band and the
 66 sharp Kondo resonance peak may be recognised as coming from a ‘constant’ term and several
 67 ‘quasiparticle-like’ excitation energies. However, the width of the Kondo peak, which is related
 68 to the Kondo temperature T_k , is exponentially small in the Coulomb interaction U , which is
 69 different from the Dirac- δ peak brought by a constant V_0 . Moreover, in the mixed valence
 70 regime, the lack of sharp peak seems to contrast with previous Vxc results from homogeneous
 71 lattice models [38,39]. Therefore, in this paper, we perform a systematic study of the symmet-
 72 ric SIAM from the perspective of the Vxc formalism. Our purpose is two-fold: i) by studying
 73 the Vxc of a QIM at finite temperature (T), we examine how the low- T thermal excitation and
 74 the inhomogeneous setup of the system are reflected in Vxc; ii) we expect to shed new light
 75 on the SIAM by investigating the real-time response of the impurity, which is not always easily
 76 accessed in conventional self-energy-based approaches. By working directly in real time, it
 77 avoids the problem of analytic continuation associated with imaginary-time approaches.

78 This paper is organized as follows. In Sec. 2, we extend the Vxc formalism, originally
 79 proposed for zero-temperature (zero- T) systems [37], to finite-temperatures (finite- T), for a
 80 temperature range of the order of the Kondo temperature T_K . This is followed by an applica-
 81 tion of the developed description to the symmetric SIAM at half-filling in Sec. 2.1. In Sec. 3, we
 82 first calculate the Vxc analytically on a dimer and numerically on a finite cluster. Based on that,
 83 we propose an ansatz for the SIAM Vxc, from which the local spectral function is obtained.
 84 Quantities such as the Kondo temperature and thermal capacity are re-interpreted within the
 85 Vxc framework. Finally, we provide our conclusive remarks and an outlook in Sec. 4.

86 2 Theory

87 We first derive the general finite- T Vxc formalism. After that, we apply it to a discrete cluster
 88 at thermal equilibrium which represents an impurity coupled with a bath. The low- T Vxc is
 89 obtained by taking the limit $T \rightarrow 0$. We will use atomic units throughout this paper.

90 For a system with chemical potential μ at finite temperature $T = 1/\beta$, the generalized
 91 time-independent Hamiltonian is

$$\hat{K} = \hat{H} - \mu\hat{N}. \quad (1)$$

92 With $\mathbf{r} = (\mathbf{r}, \sigma)$ the space-spin variable, $\hat{\psi}(\mathbf{r})$ the field operator and $\hat{\rho}(\mathbf{r})$ the density operator,
 93 we have

$$\hat{H} = \int d\mathbf{r} \hat{\psi}^\dagger(\mathbf{r}) h_0(\mathbf{r}) \hat{\psi}(\mathbf{r}) + \frac{1}{2} \int d\mathbf{r} d\mathbf{r}' \hat{\psi}^\dagger(\mathbf{r}) \hat{\psi}^\dagger(\mathbf{r}') v(\mathbf{r}, \mathbf{r}') \hat{\psi}(\mathbf{r}') \hat{\psi}(\mathbf{r}), \quad (2)$$

94 where the single-particle term $h_0(\mathbf{r}) = -\frac{1}{2}\nabla^2 + V^{\text{ext}}(\mathbf{r})$ is a sum of kinetic energy and the ex-
 95 ternal field V^{ext} , $v(\mathbf{r}, \mathbf{r}') = \frac{1}{|\mathbf{r}-\mathbf{r}'|}$ is the Coulomb interaction, and the particle-number operator
 96 reads

$$\hat{N} = \int d\mathbf{r} \hat{\psi}^\dagger(\mathbf{r}) \hat{\psi}(\mathbf{r}) = \int d\mathbf{r} \hat{\rho}(\mathbf{r}) \quad (3)$$

97 The Vxc formalism is based on the finite- T time-ordered single-particle Green’s function
 98 [41]

$$i\bar{G}(\mathbf{r}t, \mathbf{r}'t') := \langle\langle \hat{\psi}(\mathbf{r}t); \hat{\psi}^\dagger(\mathbf{r}'t') \rangle\rangle = \text{Tr}\{\hat{\rho}_G \mathcal{T}[\hat{\psi}(\mathbf{r}t) \hat{\psi}^\dagger(\mathbf{r}'t')]\} \quad (4)$$

99 where \mathcal{T} is the real-time time-ordering symbol, $\hat{\rho}_G = Z_G^{-1} e^{-\beta \hat{K}}$ the statistical operator, $Z_G = \text{Tr}[e^{-\beta \hat{K}}]$
 100 the grand canonical partition function, and $\hat{\psi}(rt) = e^{i\hat{K}t} \hat{\psi}(r) e^{-i\hat{K}t}$ and its conjugate $\hat{\psi}^\dagger$ are
 101 the Heisenberg-picture field operators. The $\langle\langle \dots \rangle\rangle$ symbol denotes the thermal ensemble aver-
 102 age of the time-ordered operators. The equation of motion of the Green's function in the Vxc
 103 scheme is

$$[i\partial_t - h(r)]\bar{G}(rt, r't') - V^{\text{xc}}(rt, r't')\bar{G}(rt, r't') = \delta(t-t')\delta(r-r'), \quad (5)$$

104 where $h(rt) = h_0(r) + V^{\text{H}}(r) - \mu$ contains the Hartree field $V^{\text{H}}(r) = \int dr' v(r, r') \text{Tr}\{\hat{\rho}_G \hat{\rho}(r')\}$.
 105 The Vxc is defined to according to:

$$V^{\text{xc}}(rt, r't') i\bar{G}(rt, r't') := \int dr'' v(r, r'') \langle\langle \hat{\rho}(r''t) \hat{\psi}(rt); \hat{\psi}^\dagger(r't') \rangle\rangle - V^{\text{H}}(r) i\bar{G}(rt, r't'). \quad (6)$$

106 A correlator g can be defined to factorize the high-order term $\langle\langle \hat{\rho}(r''t) \hat{\psi}(rt); \hat{\psi}^\dagger(r't') \rangle\rangle$
 107 [37]:

$$\langle\langle \hat{\rho}(r''t) \hat{\psi}(rt); \hat{\psi}^\dagger(r't') \rangle\rangle = i\bar{G}(rt, r't') g(r, r', r''; t, t') \rho(r''), \quad (7)$$

108 where $\rho(r'') = \text{Tr}\{\hat{\rho}_G \hat{\rho}(r'')\}$ is the ensemble average of the electron density. We can define
 109 a dynamical xc hole

$$\rho^{\text{xc}}(r, r', r''; t, t') = [g(r, r', r''; t, t') - 1] \rho(r''), \quad (8)$$

110 which fulfills a sum rule when the number of electrons is conserved (the derivation essentially
 111 follows that of the zero- T case [37] except that ground-state expectation value is replaced by
 112 thermal average)

$$\int dr'' \rho^{\text{xc}}(r, r', r''; t, t') = -\theta(t' - t). \quad (9)$$

113 Substituting the high-order term in Eq. (6) with the xc hole, the xc potential can be essentially
 114 written as

$$V^{\text{xc}}(rt, r't') = \int dr'' v(r, r'') \rho^{\text{xc}}(r, r', r''; t, t'), \quad (10)$$

115 which indicates that the finite- T xc field can be interpreted as the Coulomb potential of a
 116 finite- T xc hole. Furthermore, the xc hole fulfills an exact constraint

$$\rho^{\text{xc}}(r, r', r'' = r; t, t') = -\rho(r). \quad (11)$$

117 Here we may see an advantage of the Vxc-Framework: the definition of finite- T Vxc introduced
 118 here is a natural extension from the zero- T formalism, with ground state expectation values
 119 replaced by thermal ensemble averages. The sum rule and the exact constraint which the
 120 xc hole fulfills take the same form as the $T = 0$ case. Moreover, the time-dependence of the
 121 external field can be included in a formally straightforward way ($h(r) \rightarrow h(rt)$ in Eq. (5), thus
 122 $V^{\text{H}}(rt)$ and $\rho(rt)$ depends on time). In practice, however, Vxc can have a more complicated
 123 behavior when the system is driven by a time-dependent potential from its ground state or
 124 thermal equilibrium state. The low- T properties of the equilibrium SIAM Vxc is shown in the
 125 following section.

126 2.1 Vxc formalism for the SIAM

127 The SIAM Hamiltonian reads

$$\hat{H}_{SIAM} = \epsilon_f (\hat{n}_{f\uparrow} + \hat{n}_{f\downarrow}) + U \hat{n}_{f\uparrow} \hat{n}_{f\downarrow} + \sum_{k\sigma} \left[\epsilon_k \hat{c}_{k\sigma}^\dagger \hat{c}_{k\sigma} + (v_k \hat{f}_\sigma^\dagger \hat{c}_{k\sigma} + \text{H.c.}) \right]. \quad (12)$$

128 Here \hat{f}_σ^\dagger (\hat{f}_σ) creates (annihilates) an electron with spin σ on the impurity site, $\hat{n}_\sigma = \hat{f}_\sigma^\dagger \hat{f}_\sigma$
 129 is the corresponding number operator, $\hat{c}_{k\sigma}^\dagger$ ($\hat{c}_{k\sigma}$) creates (annihilates) a bath electron with
 130 energy ϵ_k . Furthermore, v_k is the hybridization amplitude, and ϵ_f and U are the impurity
 131 on-site energy and Coulomb interaction, respectively. We consider a symmetric SIAM at half-
 132 filling, which means $U + 2\epsilon_f = 0$, and the ensemble average $n_{f\sigma} = \text{Tr}\{\hat{\rho}_G \hat{n}_{f\sigma}\} = 0.5$. We also
 133 choose the number of fermionic sites (impurity + bath) L even. The local spectral function
 134 can be obtained from the impurity Green's function

$$\begin{aligned} i\bar{G}_{ff,\sigma}(t, \beta) &= \langle\langle \hat{f}_\sigma(t); \hat{f}_\sigma^\dagger(0) \rangle\rangle \\ &= \theta(t) \frac{\sum_{mn_+} e^{-\beta E_m} e^{-i(E_{n_+} - E_m)t} |\langle n_+ | \hat{f}_\sigma^\dagger | m \rangle|^2}{\sum_m e^{-\beta E_m}} \\ &\quad - \theta(-t) \frac{\sum_{mn_-} e^{-\beta E_m} e^{i(E_{n_-} - E_m)t} |\langle n_- | \hat{f}_\sigma | m \rangle|^2}{\sum_m e^{-\beta E_m}}, \end{aligned} \quad (13)$$

135 where we set $t' = 0$ since the system is in equilibrium, θ is the Heaviside step function, and
 136 m, n_+ and n_- label eigenstates with $L, L + 1$ and $L - 1$ electrons, respectively. The system has
 137 particle-hole symmetry, therefore we focus on the positive time, namely the particle part,

$$i\bar{G}_{ff,\sigma}^p(t > 0, \beta) = \frac{\sum_m e^{-\beta E_m} \sum_{n_+} a_{n_+,m} e^{-i\omega_{n_+,m}t}}{\sum_m e^{-\beta E_m}}, \quad (14)$$

138 where $\omega_{n_+,m} = E_{n_+} - E_m$ are the excitation energies and $a_{n_+,m} = |\langle n_+ | \hat{f}_\sigma^\dagger | m \rangle|^2$ their corre-
 139 sponding weight. The equation of motion of the Green's function reads

$$[i\partial_t - \epsilon_f - V^H - V_\sigma^{\text{xc}}(t, \beta)]\bar{G}_{ff,\sigma}(t, \beta) = \delta(t), \quad (15)$$

140 where the Hartree term $V^H = U n_{f\bar{\sigma}}$ is proportional to the density of impurity electron with
 141 opposite spin $\bar{\sigma} \neq \sigma$. Here, we emphasize that the V_{xc} is a result of the Coulomb interac-
 142 tion and can be interpreted as the Coulomb potential of the xc hole, which can be seen from
 143 Eq. (6). However, for the SIAM, the hybridization between the impurity and the bath is also
 144 a crucial factor influencing the spectral properties. A dynamical hybridization field, also di-
 145 rectly coupled to the Green's function in the equation of motion, can be defined within the
 146 V_{xc} -Framework. We incorporate the hybridization field into the V_{xc} so that the equation of
 147 motion has a simpler form, and with the given V_{xc} , the Green's function can be directly solved.
 148 To investigate the hybridization effect, we consider the noninteracting case ($U = 0$ in Eq. (12)).
 149 At zero- T , the impurity Green's function $G_{ff,\sigma}$ can be analytically solved as

$$G_{ff,\sigma}(\omega) = \frac{1}{\omega - \epsilon_f - \Delta(\omega)}, \quad (16)$$

150 where

$$\Delta(\omega) = \sum_k \frac{|v_k|^2}{\omega^+ - \epsilon_k} \quad (17)$$

151 is the hybridization function. $\Delta(\omega)$ can be calculated analytically by modeling the continuous
 152 bath as a tight-binding ring with N_c sites and hopping strength t_h , and the impurity site couples
 153 to one site with strength V (see Fig. 1). In this model, the SIAM parameters are given by
 154 $\epsilon_k = 2t_h \cos(k)$ and $v_k = \frac{V}{\sqrt{N_c}}$. When $|\epsilon_f|, V \ll 2|t_h|$, we approach the so-called wide-band
 155 limit (WBL), thus the hybridization function can be treated as a constant for $|\omega| \ll 2|t_h|$,

$$\Delta(\omega) = i\Gamma = i \frac{\pi V^2}{4t_h}. \quad (18)$$

156 Accordingly, we can solve the hybridization field:

$$V_{\text{nonint,WBL}}^{\text{xc}}(t) = i\Gamma\theta(-t). \quad (19)$$

157 The physical picture is as follows: the infinitely wide bath band leads to a broadening of
 158 the impurity level ϵ_f , which is represented by a purely imaginary hybridization field. This
 hybridization effect exists also for non-WBL or interacting cases.

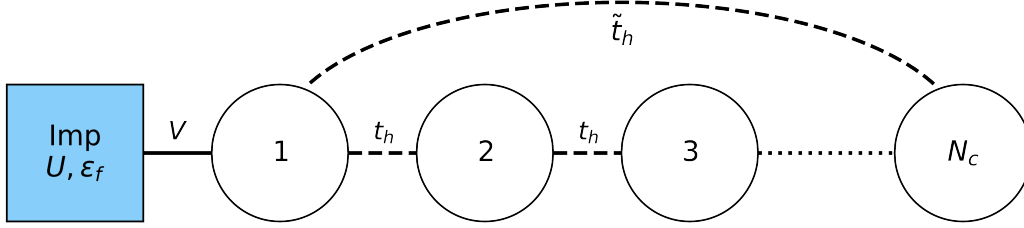


Figure 1: The 1D tight-binding system used to model an impurity coupled to a continuous bath. When periodic boundary conditions are used for the N_c noninteracting sites ($\tilde{t}_h = t_h$), we have the effective SIAM parameters $\epsilon_k = 2t_h \cos(k)$ and $v_k = \frac{V}{\sqrt{N_c}}$. When $\tilde{t}_h=0$, the model approaches the SIAM setup in the large N_c limit.

159

160 2.2 The SIAM Vxc at low-temperature

161 The Vxc coupled to $\bar{G}_{ff,\sigma}^P$ can be obtained from the equation of motion. For the symmetric
 162 SIAM at half-filling, $\epsilon_f + V^H = 0$, thus

$$V_{p,\sigma}^{\text{xc}}(t, \beta) = \frac{\sum_m e^{-\beta E_m} \sum_{n^+} a_{n^+,m} \omega_{n^+,m} e^{-i\omega_{n^+,m} t}}{\sum_m e^{-\beta E_m} \sum_{n^+} a_{n^+,m} e^{-i\omega_{n^+,m} t}}. \quad (20)$$

163 We focus on the low-temperature case (referred to as low- T) such that $e^{-\beta E_m}$ is negligible
 164 except for the lowest two eigenstates $m = 1, 2$. The Vxc can be written as (the derivation is in
 165 Appendix A)

$$V_{p,\sigma}^{\text{xc}}(t, \beta) = V_{p,\sigma}^{\text{xc}}(t, T = 0) + \tilde{V}(t) e^{-\beta(E_2 - E_1)}, \quad (21)$$

166 which is the zero temperature $V_{p,\sigma}^{\text{xc}}(t, T = 0)$ plus a correction from a time-oscillating term
 167 $\tilde{V}_{p,\sigma}(t)$ and an exponentially small factor. Both the zero- T V^{xc} and the oscillating term \tilde{V} are
 168 determined by the interaction on the impurity site and the hybridization between the impurity
 169 and the bath. In the next section, we i) calculate analytically the low- T Vxc of a dimer where
 170 the interaction is nonzero on one site and ii) present the Vxc of an SIAM on a finite cluster
 171 determined numerically. Our aim is to investigate the influence of the interaction U and the
 172 hybridization V on the Vxc, for the dimer and the cluster, respectively. We will after that
 173 propose an ansatz for the finite- T SIAM Vxc and relate the ansatz parameters to the Kondo
 174 physics in the thermodynamic limit.

175 3 Results

176 3.1 Analytic insights from a dimer

177 We use a dimer with interaction U only on one site and hopping V between the sites to derive
178 the analytic Vxc:

$$\hat{H}_{\text{dimer}} = \epsilon_f (\hat{n}_{f\uparrow} + \hat{n}_{f\downarrow}) + U \hat{n}_{f\uparrow} \hat{n}_{f\downarrow} + V \sum_{\sigma} (\hat{f}_{\sigma}^{\dagger} \hat{c}_{\sigma} + \text{H.c.}), \quad (22)$$

179 where we fix $\epsilon_f = -\frac{U}{2}$ and the dimer at half-filling. We consider the $T = 0$ case first. In the
180 Kondo regime ($U \gg V$), the particle part of Vxc has an approximate form (for the derivation,
181 see Appendix B)

$$V_{p,\sigma}^{\text{xc}}(t, T = 0) \approx \omega_p - \lambda \Omega e^{i\Omega t}, \quad (23)$$

182 where $\omega_p = \sqrt{\frac{U^2}{16} + 4V^2} + \sqrt{\frac{U^2}{16} + V^2}$, $\lambda \approx \frac{36V^2}{U^2}$, and $\Omega = \sqrt{\frac{U^2}{4} + 4V^2}$. Eq. (23) indicates that
183 the dimer Vxc, similar to the cases mentioned in Sec. 1, can be seen as a sum of a constant term
184 and a quasiparticle-like exponential term. Given the Vxc, the corresponding Green's function
185 can be obtained by solving the equation of motion,

$$\begin{aligned} \bar{G}_{ff,\sigma}^P(t, T = 0) &= \bar{G}_{ff,\sigma}^P(0^+, T = 0) e^{-i(V^H + \omega_p)t} e^{i \int_0^t \lambda \Omega e^{i\Omega \bar{t}} d\bar{t}} \\ &\approx g^+ \left[(1 - \lambda) e^{-i(\epsilon_f + V^H + \omega_p)t} + \lambda e^{-i(\epsilon_f + V^H + \omega_0)t} \right], \end{aligned} \quad (24)$$

186 where $\omega_0 = \omega_p - \Omega \sim \frac{V^2}{U}$, $g^+ = \bar{G}_{ff,\sigma}^P(0^+, T = 0)$. For the symmetric model at half-filling,
187 $g^+ = -0.5i$ and $\epsilon_f + V^H = 0$. The zero- T spectral function can be obtained with particle-hole
188 symmetry,

$$A_{\text{dimer}}(\omega, T = 0) = \frac{1 - \lambda}{2} \delta(\omega + \omega_p) + \frac{\lambda}{2} \delta(\omega + \omega_0) + \frac{\lambda}{2} \delta(\omega - \omega_0) + \frac{1 - \lambda}{2} \delta(\omega - \omega_p). \quad (25)$$

189 Despite the obvious difference in complexity between the dimer and the SIAM, some physics
190 of the SIAM can be outlined from the analytic expression of the dimer Vxc: for large U , two
191 peaks ($\omega = \pm \omega_p$) of the spectral function are present, which correspond to impurity levels
192 $\epsilon_f, \epsilon_f + U$. The excitation with energy Ω creates two central peaks at $\omega = \pm \omega_0 \approx 0$. However,
193 for the dimer the spectral weights of the central peaks, $\frac{\lambda}{2} \sim (\frac{V}{U})^2$, vanish as U increase. The
194 lack of Kondo resonance can be naturally understood as the impurity site is coupled to a single
195 site instead of a continuous bath. This is directly reflected by the Vxc: as U increases, the
196 exponential term (with amplitude $\lambda \Omega \sim \frac{V^2}{U}$) becomes negligible.

197 For low- T , the time-oscillating term in Eq. (21) can be written as

$$\frac{\tilde{V}(t)}{V_{p,\sigma}^{\text{xc}}(t, T = 0)} \approx \lambda' e^{i\Omega' t} - \lambda'' e^{i\Omega'' t}, \quad (26)$$

198 where $\lambda', \lambda'' \sim \frac{V^2}{U^2}$, $\Omega' \sim U$ and $\Omega'' \sim \frac{V^2}{U}$ (see full expressions in Eqs. (B.27), (B.28), and
199 (B.29) in Appendix B). The Vxc is then

$$V_{p,\sigma}^{\text{xc}}(t, \beta) \approx \omega_p - \lambda \Omega e^{i\Omega t} + e^{-\beta \Delta_0} \omega_p (\lambda' e^{i\Omega' t} - \lambda'' e^{i\Omega'' t}), \quad (27)$$

200 where $\Delta_0 \sim \frac{V^2}{U}$. Note that we require low temperature condition $e^{-\beta\Delta_0} \ll 1$. The particle
201 part spectral function is

$$A_{\text{dimer}}(\omega > 0, \beta) \cong \frac{1 - \lambda - e^{-\beta\Delta_0} \omega_p \left(\frac{\lambda''}{\Omega''} - \frac{\lambda'}{\Omega'} \right)}{2} \delta(\omega - \omega_p) + \frac{\lambda}{2} \delta(\omega - \omega_0) \\ + \frac{e^{-\beta\Delta_0} \omega_p \frac{\lambda''}{\Omega''}}{2} \delta(\omega - \tilde{\omega}_p) - \frac{e^{-\beta\Delta_0} \omega_p \frac{\lambda'}{\Omega'}}{2} \delta(\omega - \tilde{\omega}_0), \quad (28)$$

202 where $\tilde{\omega}_0 = \omega_p - \Omega'$ and $\tilde{\omega}_p = \omega_p - \Omega''$. The first two terms on the RHS of Eq. (28) correspond
203 to the zero- T peaks, while the last two terms, with weights proportional to $e^{-\beta\Delta_0}$, are two small
204 peaks (referred to as thermal peaks in the text below) close to the zero- T peaks, respectively.
205 The mixture of a zero- T peak and a thermal peak with close frequencies can be seen as a
206 broadening of the zero- T peak. Thus the temperature-induced broadening of the SIAM spectral
207 peaks may be explained in the Vxc picture: *at low- T , thermal fluctuations induce peaks close to*
208 *the zero- T peaks.* The energy difference between the zero- T peak and the thermal peak gives
209 effectively the width of the finite- T spectral peak.

210 3.2 Including hybridization with a finite cluster at zero- T

211 To investigate the combined effects of the interaction U and the hybridization V , we numeri-
212 cally solve the Vxc on a finite cluster (corresponding to the $\tilde{t}_h = 0$ case in Fig. 1)

$$\hat{H}_{\text{cluster}} = \epsilon_f (\hat{n}_{f\uparrow} + \hat{n}_{f\downarrow}) + U \hat{n}_{f\uparrow} \hat{n}_{f\downarrow} + V \sum_{\sigma} (\hat{f}_{\sigma}^{\dagger} \hat{c}_{1\sigma} + \text{H.c.}) + \sum_{i,\sigma}^{N_c-1} (t_h \hat{c}_{i,\sigma}^{\dagger} \hat{c}_{i+1,\sigma} + \text{H.c.}), \quad (29)$$

213 where N_c is the number of noninteracting sites. In the limit $N_c \rightarrow \infty$, we reproduce the
214 continuous bath (equivalent to $\epsilon_k = 2t_h \cos(k)$, $v_k = \frac{V}{\sqrt{N_c}}$ in Eq. (12)). We use the ITensor
215 library [42, 43] to perform the time-dependent variational principle (TDVP) [44, 45] algorithm
216 on a symmetric cluster with $L = N_c + 1 = 50$ sites at zero- T (the algorithm performs better in
217 system with open boundary conditions, hence we use a chain setup instead of a periodic one).
218 We show in Fig. 2 $\text{Re}V^{\text{xc}}(t)$ with different V values. Also, we plot $\text{Re}V^{\text{xc}}(\omega)$ to analyze the
219 excitation terms contained in the Vxc. For fixed model parameters $\epsilon_f = -2.5$, $U = 5$, $t_h = -1$,
220 $\text{Re}V^{\text{xc}}(t)$ with different V can be seen to have three main features. i) It oscillates around
221 some constant values close to $\frac{U+V}{2}$. The constant terms increase with V and correspond to the
222 sharp peaks of $\text{Re}V^{\text{xc}}(\omega)$ at $\omega = 0$. ii) The local maxima of $\text{Re}V^{\text{xc}}(t)$ are approximately equally
223 separated (e.g. for $V = 1$, the time intervals between local maximums are almost 1.85), which
224 may be described by a factor $\mathcal{A}e^{-i\omega_p t}$. The excitation energy ω_p corresponds to the peaks of
225 $\text{Re}V^{\text{xc}}(\omega)$ at $\omega \sim -3$. Both the amplitude \mathcal{A} and the energy $|\omega_p|$ decrease as V turns smaller,
226 as shown in the inset of Fig. 2 (right panel). iii) For $V = 1$, the local maximum of $\text{Re}V^{\text{xc}}(t)$
227 around $t = 1$ is much larger than other local maximal values. Correspondingly, $\text{Re}V^{\text{xc}}(\omega)$
228 exhibits non-Lorentzian structures for $\omega < -5$. Similar larger local maximum at small time
229 also exists for $V = 0.5, 0.2$. As shown in the inset of Fig. 2 (left panel), for $V = 0.5$, the local
230 maximum at $t \sim 2$ is nearly twice as large as the local maximum at $t \sim 4$. This drop in local
231 maxima suggests that ω_p may contain an imaginary part.

232 Features i) and ii) can be already found in the analytic expression of the dimer Vxc. How-
233 ever, feature iii) emerges only when the impurity is coupled to a large number of noninteracting
234 sites. Therefore, we attribute feature iii) to the hybridization effect. As mentioned in Sec. 2.1,
235 the Vxc here incorporates the hybridization field, which is a purely imaginary constant for the
236 noninteracting case in the WBL. We note that the constant term of the cluster Vxc has a very
237 small imaginary part. As a result, the spectral function exhibits sharp peaks at $\omega \sim \frac{U}{2}$, instead

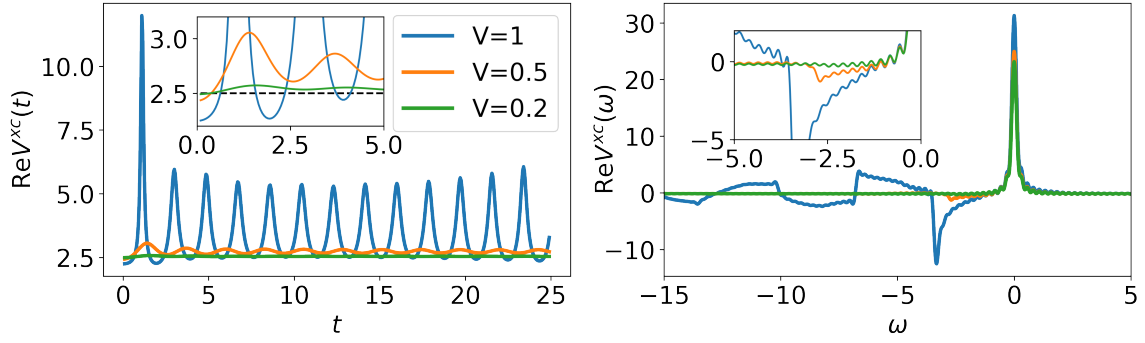


Figure 2: The Vxc of a 50-site cluster at half-filling, with parameters $\epsilon_f = -2.5, U = 5, t_h = -1, T = 0$. Left: real part of $V^{\text{xc}}(t)$. Right: real part of $V^{\text{xc}}(\omega)$, calculated with broadening factor $\eta = 0.1$.

238 of proper Hubbard side-bands. This can be attributed to the qualitative difference between
 239 the Anderson-type chain with 50 sites and the SIAM where the bath has continuous degrees
 240 of freedom.

241 To summarize the finite-cluster results, $\text{Re}V^{\text{xc}}(t)$ exhibits an oscillating behavior, which
 242 suggests that the Vxc can still take the form $V^{\text{xc}}(t) = Ae^{-i\omega_p t} + C$. However, the hybridization
 243 between the impurity and the bath requires a complex C , so that $\text{Re}C$ and $\text{Im}C$ determine the
 244 peak location and the width of the Hubbard band, respectively. Moreover, the local maxima
 245 of $\text{Re}V^{\text{xc}}(t)$ change in time, suggesting a complex ω_p .

246 3.3 Ansatz of the symmetric SIAM Vxc

247 Based on the analytic and numerical results above, we propose an ansatz for the particle part
 248 Vxc of the symmetric SIAM at low- T :

$$V^{\text{xc}}(t, \beta) = \lambda \omega_p e^{-i\omega_p t} + C, \quad (30)$$

249 where the parameters are generally temperature-dependent. λ is real, and ω_p and C are
 250 complex. The local Green's function is then approximately (see the derivation in Appendix C)

$$\bar{G}_{ff,\sigma}^p(t, \beta) = -\frac{i}{2} \left[(1-\lambda)e^{-iCt} + \lambda e^{-i(C+\omega_p)t} \right], \quad (31)$$

251 and the spectral function is

$$A(\omega > 0, \beta) = \frac{1-\lambda}{2\pi} \frac{|\text{Im}[C]|}{(\omega - \text{Re}[C])^2 + (\text{Im}[C])^2} + \frac{\lambda}{2\pi} \frac{|\text{Im}[C + \omega_p]|}{(\omega - \text{Re}[C + \omega_p])^2 + (\text{Im}[C + \omega_p])^2}. \quad (32)$$

252 Before determining the ansatz parameters numerically, we use the ansatz to interpret the
 253 Kondo spectral function. The two peaks in the spectral function can be recognized as a Hub-
 254 bard side-band located at $\omega = \text{Re}[C]$ with broadening $\text{Im}[C]$, and a Kondo peak located at
 255 $\omega = \text{Re}[C + \omega_p]$ with width $\text{Im}[C + \omega_p]$. The spectral weights of the two peaks are deter-
 256 mined by λ . The two peaks have distinct origins. The peak location and the width of the
 257 Hubbard side-band are controlled by the constant term of the Vxc, which accounts for the fact
 258 that the impurity level is affected by the interaction and broadened by the continuous bath. On
 259 the other hand, at low- T , quasiparticle-like energy ω_p creates a sharp resonance peak close
 260 to $\omega = 0$, whose width and height can be described by the Fermi-liquid treatment [46].

261 Having in mind the physical meaning of the parameters, we discuss the extrapolation proce-
 262 dure, i.e., how the ansatz quantities (λ, ω_p, C) can be calculated with a given symmetric

263 SIAM with model parameters (U, V, t_h, β) . Here, to compare with NRG results in the litera-
 264 ture (e.g., from Refs. [28] and [47]), we also use the WBL. We consider first the $T = 0$ limit,
 265 and assume that the first (second) term on the RHS of Eq. (32) contributes to the Hubbard
 266 (Kondo) peak. In this case, λ can be determined from the height of the Kondo peak:

$$\frac{\lambda}{\pi T_K} = \frac{1}{\pi \Gamma}. \quad (33)$$

267 The peak location of the Hubbard side-band can be directly calculated, which means

$$\text{Re}[\mathcal{C}] \approx \frac{U}{2}. \quad (34)$$

268 The Kondo resonance peak is at $\omega = 0$ and its width is given by the Kondo temperature
 269 (T_K) [47]. Thus,

$$\mathcal{C} + \omega_p \approx -iT_K = -i \sqrt{\frac{U\Gamma}{2}} e^{-\frac{\pi U}{8\Gamma} + \frac{\pi\Gamma}{2U}}. \quad (35)$$

270 The last unknown parameter is the imaginary part of \mathcal{C} , which corresponds to the width of the
 271 Hubbard side-band. We use the Anderson-type finite-size chain spectral function to estimate
 272 $\text{Im}[\mathcal{C}]$. Note that a finite chain cannot reproduce the proper broadening caused by an infinitely
 273 wide band. However, the relative weight between the Hubbard peak and the Kondo peak,

$$R = \frac{1 - \lambda}{2\lambda} \frac{T_k}{|\text{Im}[\mathcal{C}]|}, \quad (36)$$

274 can provide information of $\text{Im}[\mathcal{C}]$. We extrapolate the value of R by increasing the number of
 275 sites in the chain. We calculate the spectral function using the chain setup with an increas-
 276 ing number of noninteracting sites N_c . From the spectral functions (as plotted in Fig. 3a),
 277 we determine the relative weight R , which is then plotted against the total number of sites
 278 $L = N_c + 1$. For a given Γ , R increases with L (we use $L = 4, 8, 20, 30$ and 40), as shown by
 279 the scattered data points in Fig. 3b. Noticing the nearly linear increase of R at small L and
 280 expecting a converging R at large L , we fit the $R - L$ data using an hyperbolic-tangent func-
 281 tional form for the fitting function (see the curves in Fig. 3b). Consequently, $R(L = \infty)$ can
 282 be estimated using the fitting results.

283 In Fig. 4, we show the local spectral function of a symmetric SIAM in the WBL with
 284 $U = 3, t_h = 50, T = 0$. We choose the parameters ($\Gamma = 0.2, 0.5$, and 0.9) to compare with
 285 NRG results in the WBL (see Fig. 3 in Ref. [28]). The spectral function show satisfactory
 286 agreements to the NRG results. We attribute this to the fact that the Vxc as an effective field
 287 captures the intrinsic physics of an impurity problem. A complex excitation ω_p dominates the
 288 temporal behavior of the Vxc. Specifically, $\text{Re}[\omega_p] = -\frac{U}{2}$ creates the Kondo resonance peak
 289 which requires no energy transfer, and $\text{Im}[\omega_p]$ contains the Kondo temperature. At zero- T and
 290 in the WBL, most of the ansatz parameters can naturally be determined based on some well-
 291 known results of the SIAM. Only one parameter requires a numerical extrapolation. Moreover,
 292 the cluster spectral function used in the extrapolation (obtained via ED or TDVP) is actually
 293 distinct from the SIAM spectral function: for cluster results, the Kondo peak position is not at
 294 $\omega = 0$, and the Hubbard band is too sharp. As already noted close to the end of section 3.2,
 295 the discrepancy can be attributed to the essential differences between a finite cluster with tens
 296 of sites and a continuous bath. However, the Vxc scheme produces favourable spectral func-
 297 tions using these finite cluster results. This indicates that the Vxc formalism, originating from
 298 very fundamental physics and using established knowledge of the target system as a reference,
 299 is able to capture the key features of the impurity problem.

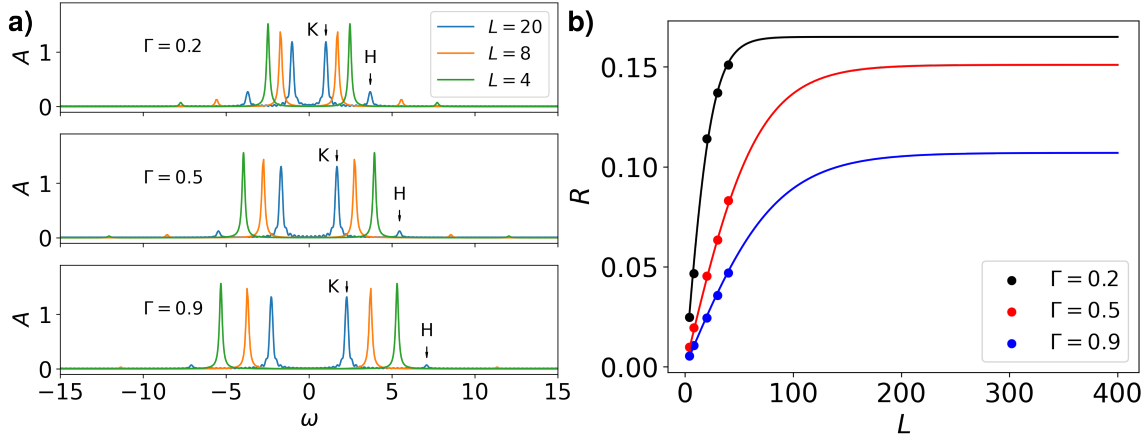


Figure 3: **a)** The zero- T spectral function of L -site clusters. We use $U = 3$, $t_h = 50$ to approach the WBL, and different V values to reach $\Gamma = 0.2, 0.5$ and 0.9 . The results are from ED for $L = 4, 8$ and from TDVP for $L = 20$. The Kondo peaks and Hubbard peaks are highlighted by arrows. **b)** The relative weight R between the Hubbard peak and the Kondo peak, as a function of the total number of sites L . TDVP is used for $L = 20, 30$ and 40 . For each value of Γ , the data are fitted using $R = R_\infty \tanh(aL)$, where R_∞ is the converged value and a is a parameter determining the converging speed. The fitted values are $R_\infty = 0.165, 0.151$, and 0.107 for $\Gamma = 0.2, 0.5$, and 0.9 , respectively.

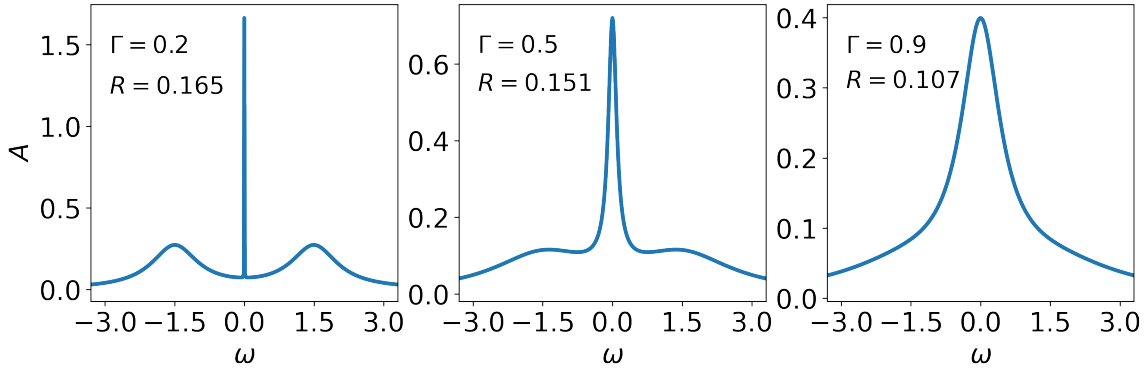


Figure 4: The zero- T spectral function of a symmetric SIAM. We use $U = 3$, $t_h = 50$ to approach the WBL, and different V values to realize desired Γ values. From the extrapolation, we get $\text{Im}[C] = -0.6, -1.3$ and -1.7 , respectively, for $\Gamma = 0.2, 0.5$ and 0.9 .

300 Lastly, we discuss the spectral function at finite temperatures, and in the range $T \in (0, T_K)$.
 301 In the Vxc formalism, we can see from the dimer result that thermal excitation leads to the
 302 broadening of both the Kondo peak and the Hubbard side-band peak. In the WBL, this thermal
 303 broadening can be effectively described by the temperature-dependence of the imaginary part
 304 of the excitation energy ω_p , while keeping other parameters temperature-independent:

$$\omega_p(T) = \omega_p(T=0) + i\Omega_T, \quad (37)$$

305 where Ω_T is much smaller than $\text{Im}[C]$. Effectively, the Hubbard side-band stays almost un-
 306 changed with the increasing T . We perform ED on an eight-site cluster with $t_h = 500$, $U = 1$
 307 and $\Gamma = 0.04$ to calculate the spectral function at $T/T_K = 0.01, 0.1, 1$. Ω_T is estimated using
 308 the position of the thermal peak nearest to the Kondo peak. Other parameters are estimated

309 using the zero- T TDVP approach. The low- T spectral function results are shown in Fig 5.
 310 Compared with NRG results (see page 3.15 of Ref. [47]), the finite- T Vxc result captures the
 311 correct trend of the Kondo peak width: at $T \ll T_K$, the contribution of Ω_T is negligible, leading
 to a width dominated by the Kondo temperature. As T approaches T_K , $|\Omega_T|$ increases .

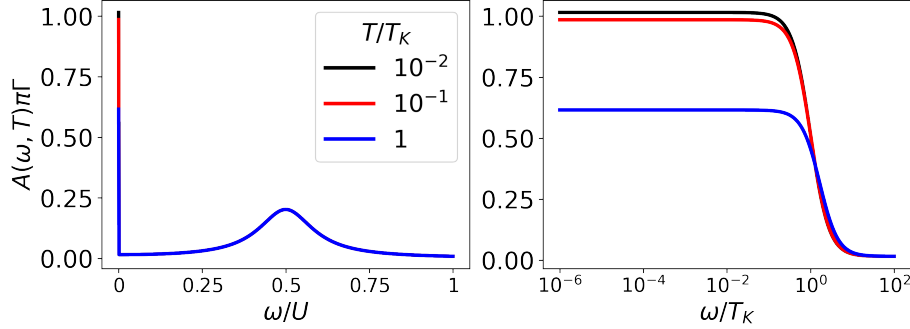


Figure 5: The spectral function of a symmetric SIAM with $t_h = 500$, $U = 2$ and $\Gamma = 0.04$, at $T = 0.01T_K$, $0.1T_K$ and T_K . Left: The frequency is in unit of U . Right: The frequency is in unit of T_K and in logarithmic scale to highlight the width of the Kondo resonance peak.

312

313 4 Conclusions and outlook

314 In this work, we applied the exchange-correlation (xc) field formalism to the symmetric single
 315 impurity Anderson model (SIAM) at low temperatures. The formalism introduces a dynamical
 316 xc field (Vxc), which can be interpreted as the Coulomb potential of the xc hole. For the
 317 SIAM, the Vxc also incorporates the hybridization effect between the impurity and the bath.
 318 We proposed an ansatz for the SIAM Vxc, which includes a complex constant term, \mathcal{C} , and a
 319 complex quasiparticle-like excitation, ω_p . The real and imaginary parts of \mathcal{C} correspond to
 320 the peak location and the width of the Hubbard side-band, respectively. More importantly,
 321 $\text{Im}[\omega_p]$ accounts for the Kondo temperature. At zero- T in the WBL, most parameters of the
 322 ansatz can be calculated from the model parameters using Fermi-liquid theory. The only un-
 323 known parameter can be estimated by an extrapolation procedure. For low temperatures, the
 324 temperature-dependence of the ansatz parameters is primarily through $\text{Im}[\omega_p]$, which again
 325 needs to be approximated numerically, guided by the insights from the auxiliary analytically
 326 dimer Vxc. Overall, the spectral function calculated from the Vxc shows satisfactory agreement
 327 with the NRG results. The extrapolation procedures involved are of low computational cost.
 328 We understand the favourable performance of the xc field formalism as follows: the screening
 329 effect underlying the SIAM is essential for the Kondo effect, and the xc field provides a suitable
 330 description for quasiparticle-like excitations. Hence, the parameters in the ansatz have clear
 331 physical meaning and can be related in a novel perspective to key well-understood features of
 332 the spectral function. The fact that only a few parameters require numerical treatment leads
 333 to a good trade-off between accuracy and computational effort.

334 As an outlook, QIMs beyond the symmetric SIAM at half-filling can also be interpreted
 335 from the perspective of the xc field formalism. We have already noted that the narrow band
 336 SIAM Vxc requires a different extrapolation scheme. Additionally, when an external magnetic
 337 field is included, the spectral function becomes spin-dependent, and the Kondo resonance can
 338 be suppressed with increasing field. In future work, we plan to investigate how the magnetic
 339 field affects the Vxc. Moreover, quantities such as the dynamical spin susceptibility, the specific
 340 heat, and the size of the Kondo cloud are related to spin correlators. We expect the spin xc

341 field formalism can be applied to these problems.

342 Finally, we stress a significant feature of the xc field formalism: it manages to reduce a
 343 complicated many-body problem to an extrapolation procedure. The extrapolation is usually
 344 done with a (numerically) solvable finite cluster or a homogeneous system as a reference.
 345 When the target system and the reference system exhibit explicit similarities, the extrapolation
 346 can be done straightforwardly. In practice, the connection between the reference system and
 347 the complex target is often less obvious. An example is the SIAM presented in this paper, where
 348 the finite cluster spectral function differs qualitatively from the SIAM. Despite this, the xc field
 349 formalism successfully captures the implicit correspondence, specifically the relative weight
 350 between the Hubbard peak and the Kondo peak at $T = 0$. Hence, we believe that the xc field
 351 formalism, based on the quasiparticle picture, is a viable and powerful approach for modeling
 352 correlated many-body system and holds great potential for first-principles calculations.

353 Acknowledgements

354 I would like to thank Ferdi Aryasetiawan and Claudio Verdozzi for stimulating discussions,
 355 reading the manuscript and providing useful comments.

356 **Funding information** I acknowledge support from the Swedish Research Council (grants
 357 number 2017-03945 and 2022-04486).

358 A Low temperature approximation of the Vxc

359 From Eq. (20) and $e^{-\beta E_m} \ll 1$ for $m > 2$, the Vxc can be written as

$$V_{p,\sigma}^{\text{xc}}(t, \beta) = \frac{C + e^{-\beta \Delta_0} D}{A + e^{-\beta \Delta_0} B}, \quad (\text{A.1})$$

360 where

$$\Delta_0 = E_2 - E_1, \quad (\text{A.2})$$

$$A = \sum_{n^+} a_{n^+,1} e^{-i\omega_{n^+,1}t}, \quad (\text{A.3})$$

$$B = \sum_{n^+} a_{n^+,2} e^{-i\omega_{n^+,2}t}, \quad (\text{A.4})$$

$$C = \sum_{n^+} a_{n^+,1} \omega_{n^+,1} e^{-i\omega_{n^+,1}t}, \quad (\text{A.5})$$

$$D = \sum_{n^+} a_{n^+,2} \omega_{n^+,2} e^{-i\omega_{n^+,2}t}. \quad (\text{A.6})$$

361 An expansion

$$\frac{1}{A + e^{-\beta \Delta_0} B} \approx \frac{1 - e^{-\beta \Delta_0} \frac{B}{A}}{A} \quad (\text{A.7})$$

362 leads to

$$V_{p,\sigma}^{\text{xc}}(t, \beta) = \frac{C}{A} + \left[\frac{D}{A} - \frac{BC}{A^2} \right] e^{-\beta \Delta_0}, \quad (\text{A.8})$$

363 where C/A is just the zero- T Vxc, and all terms of order $\mathcal{O}(e^{-\beta\Delta})$ where $\Delta > \Delta_0$ are neglected
 364 for low- T . The time-oscillating term in the main text is then

$$\tilde{V}(t) = \frac{D}{A} - \frac{BC}{A^2} = \frac{C}{A} \left[\frac{D}{C} - \frac{B}{A} \right] \quad (\text{A.9})$$

365 B Analytic Vxc of an impurity-free-electron dimer

366 We use a dimer consisting of an interacting site (f) and a noninteracting site (c) to calculate
 367 the analytic Vxc for the f site. Here we repeat the Hamiltonian in the main text:

$$\hat{H}_{\text{dimer}} = \epsilon_f(\hat{n}_{f\uparrow} + \hat{n}_{f\downarrow}) + U\hat{n}_{f\uparrow}\hat{n}_{f\downarrow} + V \sum_{\sigma} (\hat{f}_{\sigma}^{\dagger} \hat{c}_{\sigma} + \text{H.c.}), \quad (\text{B.1})$$

368 where $\epsilon_f = -\frac{U}{2}$, V is the hopping strength and the dimer is at half-filling. With variables
 369 depending on U, V

$$u = \frac{U}{2V} \quad (\text{B.2})$$

$$x = \frac{u}{4} + \sqrt{1 + \left(\frac{u}{4}\right)^2} \quad (\text{B.3})$$

$$y = \frac{u}{2} + \sqrt{1 + \left(\frac{u}{2}\right)^2}, \quad (\text{B.4})$$

370 and the same low- T assumption, the particle part of the Green's function can be written as

$$i\bar{G}_{ff,\sigma}^p(t) = Z^{-1} \left[[a_{1,1}e^{-i\omega_{1,1}t} + a_{2,1}e^{-i\omega_{2,1}t}] + e^{\beta u} [a_{1,2}e^{-i\omega_{1,2}t} + a_{2,2}e^{-i\omega_{2,2}t}] \right] \quad (\text{B.5})$$

371 where the partition function is

$$Z = 1 + 3e^{\beta(u-2x)V}, \quad (\text{B.6})$$

372 the spectral weights are

$$a_{1,1} = \frac{(x+y)^2}{2(1+x^2)(1+y^2)} \quad (\text{B.7})$$

$$a_{2,1} = \frac{(1-xy)^2}{2(1+x^2)(1+y^2)} \quad (\text{B.8})$$

$$a_{1,2} = \frac{3}{2(1+y^2)} \quad (\text{B.9})$$

$$a_{2,2} = \frac{3y^2}{2(1+y^2)}, \quad (\text{B.10})$$

373 and the excitation energies are

$$\omega_{1,1} = (2x-y)V \quad (\text{B.11})$$

$$\omega_{2,1} = (2x+y-u)V \quad (\text{B.12})$$

$$\omega_{1,2} = (-y+u)V \quad (\text{B.13})$$

$$\omega_{2,2} = yV. \quad (\text{B.14})$$

374 Following the notations in Appendix A, the zero- T V_{xc} is

$$V_{p,\sigma}^{xc}(t, T=0) = \frac{a_{1,1}\omega_{1,1}e^{-i\omega_{1,1}t} + a_{2,1}\omega_{2,1}e^{-i\omega_{2,1}t}}{a_{1,1}e^{-i\omega_{1,1}t} + a_{2,1}e^{-i\omega_{2,1}t}}. \quad (\text{B.15})$$

375 We note that in the Kondo regime ($u \gg 1$),

$$x = \frac{u}{2} + \frac{2}{u} + \mathcal{O}\left(\frac{1}{u^3}\right) \quad (\text{B.16})$$

$$y = u + \frac{1}{u} + \mathcal{O}\left(\frac{1}{u^3}\right), \quad (\text{B.17})$$

376 thus

$$\lambda := \frac{a_{1,1}}{a_{2,1}} = \frac{9}{u^2} + \mathcal{O}\left(\frac{1}{u^3}\right) \ll 1. \quad (\text{B.18})$$

377 The expansion of V_{xc} to the first order in λ gives

$$V_{p,\sigma}^{xc}(t, T=0) \approx \omega_{2,1} - \lambda \Omega e^{i\Omega t}, \quad (\text{B.19})$$

378 where

$$\Omega = \omega_{2,1} - \omega_{1,1} = \sqrt{u^2 + 4}V. \quad (\text{B.20})$$

379 For low- T , following Eq. (A.9), we have

$$\frac{\tilde{V}(t)}{V_{p,\sigma}^{xc}(t, T=0)} = \frac{a_{1,2}\omega_{1,2}e^{-i\omega_{1,2}t} + a_{2,2}\omega_{2,2}e^{-i\omega_{2,2}t}}{a_{1,1}\omega_{1,1}e^{-i\omega_{1,1}t} + a_{2,1}\omega_{2,1}e^{-i\omega_{2,1}t}} - \frac{a_{1,2}e^{-i\omega_{1,2}t} + a_{2,2}e^{-i\omega_{2,2}t}}{a_{1,1}e^{-i\omega_{1,1}t} + a_{2,1}e^{-i\omega_{2,1}t}}. \quad (\text{B.21})$$

380 Noting that for $u \gg 1$,

$$\frac{a_{1,2}}{a_{2,1}} = \frac{3}{u^2} + \mathcal{O}\left(\frac{1}{u^3}\right), \quad (\text{B.22})$$

$$\frac{a_{2,2}}{a_{2,1}} = 3\left(1 + \frac{4}{u^2}\right) + \mathcal{O}\left(\frac{1}{u^3}\right), \quad (\text{B.23})$$

$$\frac{\omega_{1,1}}{\omega_{2,1}} = \frac{3}{u^2} + \mathcal{O}\left(\frac{1}{u^3}\right), \quad (\text{B.24})$$

$$\frac{\omega_{1,2}}{\omega_{2,1}} = -\frac{1}{u^2} + \mathcal{O}\left(\frac{1}{u^3}\right), \quad (\text{B.25})$$

$$\frac{\omega_{2,2}}{\omega_{2,1}} = 1 - \frac{4}{u^2} + \mathcal{O}\left(\frac{1}{u^3}\right), \quad (\text{B.26})$$

381 we get

$$\frac{\tilde{V}(t)}{V_{p,\sigma}^{xc}(t, T=0)} = \frac{24}{u^2}e^{i\Omega't} - \frac{12}{u^2}e^{i\Omega''t} + \mathcal{O}\left(\frac{1}{u^3}\right), \quad (\text{B.27})$$

382 where

$$\Omega' = \omega_{2,1} - \omega_{1,2} = \left(\sqrt{\frac{u^2}{4} + 4} + \sqrt{u^2 + 4} - \frac{u}{2}\right)V \quad (\text{B.28})$$

$$\Omega'' = \omega_{2,1} - \omega_{2,2} = \left(\sqrt{\frac{u^2}{4} + 4} - \frac{u}{2}\right)V. \quad (\text{B.29})$$

383 The temperature factor

$$e^{-\beta\Delta_0} = e^{-\beta(2x-u)} \quad (\text{B.30})$$

384 need to be small in order for the approximation Eq. (A.7) holds.

385 C Solving the Green's function from the ansatz of the Vxc

386 For the SIAM, the equation of motion of the particle Green's function reads

$$[i\partial_t - \epsilon_f - V^H - V_{p,\sigma}^{\text{xc}}(t, \beta)]\bar{G}_{ff,\sigma}^P(t, \beta) = 0, \quad (\text{C.1})$$

387 where $\epsilon_f + V^H = 0$ and $g^+ = \bar{G}_{ff,\sigma}^P(t = 0^+, \beta) = -0.5i$ for the symmetric SIAM. Accordingly,
388 the Green's function is

$$\bar{G}_{ff,\sigma}^P(t, \beta) = g^+ e^{-i \int_0^t V_{p,\sigma}^{\text{xc}}(\bar{t}, \beta) d\bar{t}} \quad (\text{C.2})$$

389 The Vxc is

$$V_{p,\sigma}^{\text{xc}}(t, \beta) = \lambda \omega_p e^{-i\omega_p t} + \mathcal{C} \quad (\text{C.3})$$

390 where λ is real, ω_p and \mathcal{C} are complex. We have

$$\begin{aligned} e^{-i \int_0^t V_{p,\sigma}^{\text{xc}}(\bar{t}, \beta) d\bar{t}} &= e^{-i\mathcal{C}t} e^{\lambda(e^{-i\omega_p t} - 1)} \\ &\approx e^{-i\mathcal{C}t} [1 + \lambda(e^{-i\omega_p t} - 1)], \end{aligned} \quad (\text{C.4})$$

391 where we assume a small λ in the last line to get a simpler expression. The Green's function
392 is then

$$\bar{G}_{ff,\sigma}^P(t, \beta) = g^+ [(1 - \lambda)e^{-i\mathcal{C}t} + \lambda e^{-i(\mathcal{C} + \omega_p)t}]. \quad (\text{C.5})$$

393 References

- 394 [1] A. C. Hewson, *The Kondo Problem to Heavy Fermions*, Cambridge Studies in Magnetism.
395 Cambridge University Press (1993).
- 396 [2] Y. Meir, N. S. Wingreen and P. A. Lee, *Low-temperature transport through a quan-*
397 *tum dot: The anderson model out of equilibrium*, Phys. Rev. Lett. **70**, 2601 (1993),
398 doi:[10.1103/PhysRevLett.70.2601](https://doi.org/10.1103/PhysRevLett.70.2601).
- 399 [3] D. Goldhaber-Gordon, H. Shtrikman, D. Mahalu, D. Abusch-Magder, U. Meirav and
400 M. A. Kastner, *Kondo effect in a single-electron transistor*, Nature **391**, 156 (1998),
401 doi:[10.1038/34373](https://doi.org/10.1038/34373).
- 402 [4] S. M. Cronenwett, T. H. Oosterkamp and L. P. Kouwenhoven, *A Tunable Kondo Effect in*
403 *Quantum Dots*, Science **281**(5376), 540 (1998), doi:[10.1126/science.281.5376.540](https://doi.org/10.1126/science.281.5376.540),
404 <https://www.science.org/doi/pdf/10.1126/science.281.5376.540>.
- 405 [5] V. Madhavan, W. Chen, T. Jamneala, M. F. Crommie and N. S. Wingreen, *Tunneling into a*
406 *Single Magnetic Atom: Spectroscopic Evidence of the Kondo Resonance*, Science **280**(5363),
407 567 (1998), doi:[10.1126/science.280.5363.567](https://doi.org/10.1126/science.280.5363.567), [https://www.science.org/doi/pdf/10.](https://www.science.org/doi/pdf/10.1126/science.280.5363.567)
408 [1126/science.280.5363.567](https://www.science.org/doi/pdf/10.1126/science.280.5363.567).
- 409 [6] J. Li, W.-D. Schneider, R. Berndt and B. Delley, *Kondo Scattering Observed at a Single*
410 *Magnetic Impurity*, Phys. Rev. Lett. **80**, 2893 (1998), doi:[10.1103/PhysRevLett.80.2893](https://doi.org/10.1103/PhysRevLett.80.2893).
- 411 [7] O. Újsághy, J. Kroha, L. Szunyogh and A. Zawadowski, *Theory of the Fano Resonance in*
412 *the STM Tunneling Density of States due to a Single Kondo Impurity*, Phys. Rev. Lett. **85**,
413 2557 (2000), doi:[10.1103/PhysRevLett.85.2557](https://doi.org/10.1103/PhysRevLett.85.2557).

- 414 [8] L. Amico, R. Fazio, A. Osterloh and V. Vedral, *Entanglement in many-body systems*, Rev.
415 Mod. Phys. **80**, 517 (2008), doi:[10.1103/RevModPhys.80.517](https://doi.org/10.1103/RevModPhys.80.517).
- 416 [9] P. Samuelsson and C. Verdozzi, *Two-particle spin entanglement in magnetic anderson nan-*
417 *oclusters*, Phys. Rev. B **75**, 132405 (2007), doi:[10.1103/PhysRevB.75.132405](https://doi.org/10.1103/PhysRevB.75.132405).
- 418 [10] P. W. Anderson, *Localized Magnetic States in Metals*, Phys. Rev. **124**, 41 (1961),
419 doi:[10.1103/PhysRev.124.41](https://doi.org/10.1103/PhysRev.124.41).
- 420 [11] A. Georges, G. Kotliar, W. Krauth and M. J. Rozenberg, *Dynamical mean-field theory of*
421 *strongly correlated fermion systems and the limit of infinite dimensions*, Rev. Mod. Phys.
422 **68**, 13 (1996), doi:[10.1103/RevModPhys.68.13](https://doi.org/10.1103/RevModPhys.68.13).
- 423 [12] S. Biermann, F. Aryasetiawan and A. Georges, *First-Principles Approach to the*
424 *Electronic Structure of Strongly Correlated Systems: Combining the GW Approx-*
425 *imation and Dynamical Mean-Field Theory*, Phys. Rev. Lett. **90**, 086402 (2003),
426 doi:[10.1103/PhysRevLett.90.086402](https://doi.org/10.1103/PhysRevLett.90.086402).
- 427 [13] G. Kotliar, S. Y. Savrasov, K. Haule, V. S. Oudovenko, O. Parcollet and C. A. Marianetti,
428 *Electronic structure calculations with dynamical mean-field theory*, Rev. Mod. Phys. **78**,
429 865 (2006), doi:[10.1103/RevModPhys.78.865](https://doi.org/10.1103/RevModPhys.78.865).
- 430 [14] H. Aoki, N. Tsuji, M. Eckstein, M. Kollar, T. Oka and P. Werner, *Nonequilibrium*
431 *dynamical mean-field theory and its applications*, Rev. Mod. Phys. **86**, 779 (2014),
432 doi:[10.1103/RevModPhys.86.779](https://doi.org/10.1103/RevModPhys.86.779).
- 433 [15] K. G. Wilson, *The renormalization group: Critical phenomena and the Kondo problem*, Rev.
434 Mod. Phys. **47**, 773 (1975), doi:[10.1103/RevModPhys.47.773](https://doi.org/10.1103/RevModPhys.47.773).
- 435 [16] E. Gull, A. J. Millis, A. I. Lichtenstein, A. N. Rubtsov, M. Troyer and P. Werner, *Continuous-*
436 *time Monte Carlo methods for quantum impurity models*, Rev. Mod. Phys. **83**, 349 (2011),
437 doi:[10.1103/RevModPhys.83.349](https://doi.org/10.1103/RevModPhys.83.349).
- 438 [17] N. Andrei, K. Furuya and J. H. Lowenstein, *Solution of the Kondo problem*, Rev. Mod.
439 Phys. **55**, 331 (1983), doi:[10.1103/RevModPhys.55.331](https://doi.org/10.1103/RevModPhys.55.331).
- 440 [18] P. B. Wiegmann and A. M. Tsvelick, *Exact solution of the Anderson model: I*, J. Phys. C:
441 Solid State Phys. **16**(12), 2281 (1983), doi:[10.1088/0022-3719/16/12/017](https://doi.org/10.1088/0022-3719/16/12/017).
- 442 [19] A. M. Tsvelick and P. B. Wiegmann, *Exact solution of the Anderson model. II. Thermody-*
443 *namical properties at finite temperatures*, J. Phys. C: Solid State Phys. **16**(12), 2321 (1983),
444 doi:[10.1088/0022-3719/16/12/018](https://doi.org/10.1088/0022-3719/16/12/018).
- 445 [20] W. Hofstetter, *Generalized Numerical Renormalization Group for Dynamical Quantities*,
446 Phys. Rev. Lett. **85**, 1508 (2000), doi:[10.1103/PhysRevLett.85.1508](https://doi.org/10.1103/PhysRevLett.85.1508).
- 447 [21] R. Peters, T. Pruschke and F. B. Anders, *Numerical renormalization group approach*
448 *to green's functions for quantum impurity models*, Phys. Rev. B **74**, 245114 (2006),
449 doi:[10.1103/PhysRevB.74.245114](https://doi.org/10.1103/PhysRevB.74.245114).
- 450 [22] A. Weichselbaum and J. von Delft, *Sum-Rule Conserving Spectral Functions from*
451 *the Numerical Renormalization Group*, Phys. Rev. Lett. **99**, 076402 (2007),
452 doi:[10.1103/PhysRevLett.99.076402](https://doi.org/10.1103/PhysRevLett.99.076402).
- 453 [23] i. c. v. Osolin and R. Žitko, *Padé approximant approach for obtaining finite-temperature*
454 *spectral functions of quantum impurity models using the numerical renormalization group*
455 *technique*, Phys. Rev. B **87**, 245135 (2013), doi:[10.1103/PhysRevB.87.245135](https://doi.org/10.1103/PhysRevB.87.245135).

- 456 [24] A. Isidori, D. Roosen, L. Bartosch, W. Hofstetter and P. Kopietz, *Spectral function of*
457 *the Anderson impurity model at finite temperatures*, Phys. Rev. B **81**, 235120 (2010),
458 doi:[10.1103/PhysRevB.81.235120](https://doi.org/10.1103/PhysRevB.81.235120).
- 459 [25] A. Ge, N. Ritz, E. Walter, S. Aguirre, J. von Delft and F. B. Kugler, *Real-frequency quantum*
460 *field theory applied to the single-impurity Anderson model*, Phys. Rev. B **109**, 115128
461 (2024), doi:[10.1103/PhysRevB.109.115128](https://doi.org/10.1103/PhysRevB.109.115128).
- 462 [26] D. Zgid, E. Gull and G. K.-L. Chan, *Truncated configuration interaction expansions as*
463 *solvers for correlated quantum impurity models and dynamical mean-field theory*, Phys.
464 Rev. B **86**, 165128 (2012), doi:[10.1103/PhysRevB.86.165128](https://doi.org/10.1103/PhysRevB.86.165128).
- 465 [27] M. Granath and H. U. R. Strand, *Distributional exact diagonalization for-*
466 *malism for quantum impurity models*, Phys. Rev. B **86**, 115111 (2012),
467 doi:[10.1103/PhysRevB.86.115111](https://doi.org/10.1103/PhysRevB.86.115111).
- 468 [28] S. Motahari, R. Requist and D. Jacob, *Kondo physics of the Anderson impurity*
469 *model by distributional exact diagonalization*, Phys. Rev. B **94**, 235133 (2016),
470 doi:[10.1103/PhysRevB.94.235133](https://doi.org/10.1103/PhysRevB.94.235133).
- 471 [29] G. Stefanucci and S. Kurth, *Steady-State Density Functional Theory for Finite Bias Conduc-*
472 *tances*, Nano Letters **15**(12), 8020 (2015), doi:[10.1021/acs.nanolett.5b03294](https://doi.org/10.1021/acs.nanolett.5b03294), PMID:
473 26571349, <https://doi.org/10.1021/acs.nanolett.5b03294>.
- 474 [30] S. Kurth and G. Stefanucci, *Nonequilibrium Anderson model made simple with density*
475 *functional theory*, Phys. Rev. B **94**, 241103 (2016), doi:[10.1103/PhysRevB.94.241103](https://doi.org/10.1103/PhysRevB.94.241103).
- 476 [31] D. Jacob and S. Kurth, *Many-Body Spectral Functions from Steady State Density Functional*
477 *Theory*, Nano Letters **18**(3), 2086 (2018), doi:[10.1021/acs.nanolett.8b00255](https://doi.org/10.1021/acs.nanolett.8b00255), PMID:
478 29437404, <https://doi.org/10.1021/acs.nanolett.8b00255>.
- 479 [32] P. Kubiczek, A. N. Rubtsov and A. I. Lichtenstein, *Exact real-time dynamics of single-*
480 *impurity Anderson model from a single-spin hybridization-expansion*, SciPost Phys. **7**, 016
481 (2019), doi:[10.21468/SciPostPhys.7.2.016](https://doi.org/10.21468/SciPostPhys.7.2.016).
- 482 [33] A. J. Kim, J. Li, M. Eckstein and P. Werner, *Pseudoparticle vertex solver for quantum*
483 *impurity models*, Phys. Rev. B **106**, 085124 (2022), doi:[10.1103/PhysRevB.106.085124](https://doi.org/10.1103/PhysRevB.106.085124).
- 484 [34] D. Werner, J. Lotze and E. Arrigoni, *Configuration interaction based nonequi-*
485 *librium steady state impurity solver*, Phys. Rev. B **107**, 075119 (2023),
486 doi:[10.1103/PhysRevB.107.075119](https://doi.org/10.1103/PhysRevB.107.075119).
- 487 [35] N. Ng, G. Park, A. J. Millis, G. K.-L. Chan and D. R. Reichman, *Real-time evolution of*
488 *Anderson impurity models via tensor network influence functionals*, Phys. Rev. B **107**,
489 125103 (2023), doi:[10.1103/PhysRevB.107.125103](https://doi.org/10.1103/PhysRevB.107.125103).
- 490 [36] B. Kloss, J. Thoenniss, M. Sonner, A. Lerose, M. T. Fishman, E. M. Stoudenmire, O. Par-
491 collet, A. Georges and D. A. Abanin, *Equilibrium quantum impurity problems via ma-*
492 *trix product state encoding of the retarded action*, Phys. Rev. B **108**, 205110 (2023),
493 doi:[10.1103/PhysRevB.108.205110](https://doi.org/10.1103/PhysRevB.108.205110).
- 494 [37] F. Aryasetiawan, *Time-dependent exchange-correlation potential in lieu of self-energy*, Phys.
495 Rev. B **105**, 075106 (2022), doi:[10.1103/PhysRevB.105.075106](https://doi.org/10.1103/PhysRevB.105.075106).

- 496 [38] F. Aryasetiawan and T. Sjöstrand, *Spectral functions of the half-filled one-dimensional*
497 *Hubbard chain within the exchange-correlation potential formalism*, Phys. Rev. B **106**,
498 045123 (2022), doi:[10.1103/PhysRevB.106.045123](https://doi.org/10.1103/PhysRevB.106.045123).
- 499 [39] Z. Zhao, C. Verdozzi and F. Aryasetiawan, *Dynamical exchange-correlation potential for-*
500 *malism for spin- $\frac{1}{2}$ Heisenberg and Hubbard chains: The antiferromagnetic/half-filled case*,
501 Phys. Rev. B **108**, 235132 (2023), doi:[10.1103/PhysRevB.108.235132](https://doi.org/10.1103/PhysRevB.108.235132).
- 502 [40] K. Karlsson and F. Aryasetiawan, *Time-dependent exchange-correlation hole*
503 *and potential of the electron gas*, Phys. Rev. B **107**, 115172 (2023),
504 doi:[10.1103/PhysRevB.107.115172](https://doi.org/10.1103/PhysRevB.107.115172).
- 505 [41] A. L. Fetter and J. D. Walecka, *Quantum Theory of Many-Particle Systems*, Courier Cor-
506 poration (2012).
- 507 [42] M. Fishman, S. R. White and E. M. Stoudenmire, *The ITensor Software Li-*
508 *brary for Tensor Network Calculations*, SciPost Phys. Codebases p. 4 (2022),
509 doi:[10.21468/SciPostPhysCodeb.4](https://doi.org/10.21468/SciPostPhysCodeb.4).
- 510 [43] M. Fishman, S. R. White and E. M. Stoudenmire, *Codebase release 0.3 for ITensor*, SciPost
511 Phys. Codebases pp. 4–r0.3 (2022), doi:[10.21468/SciPostPhysCodeb.4-r0.3](https://doi.org/10.21468/SciPostPhysCodeb.4-r0.3).
- 512 [44] J. Haegeman, J. I. Cirac, T. J. Osborne, I. Pižorn, H. Verschelde and F. Verstraete, *Time-*
513 *Dependent Variational Principle for Quantum Lattices*, Phys. Rev. Lett. **107**, 070601
514 (2011), doi:[10.1103/PhysRevLett.107.070601](https://doi.org/10.1103/PhysRevLett.107.070601).
- 515 [45] M. Yang and S. R. White, *Time-dependent variational principle with ancillary Krylov sub-*
516 *space*, Phys. Rev. B **102**, 094315 (2020), doi:[10.1103/PhysRevB.102.094315](https://doi.org/10.1103/PhysRevB.102.094315).
- 517 [46] P. Nozières, *A “fermi-liquid” description of the Kondo problem at low temperatures*, J. Low
518 Temp. Phys. **17** (1974), doi:[10.1007/BF00654541](https://doi.org/10.1007/BF00654541).
- 519 [47] E. Pavarini, E. Koch, A. Lichtenstein and D. Vollhardt, eds., *Dynamical Mean-Field Theory*
520 *of Correlated Electrons: Modeling and Simulation*, Verlag des Forschungszentrum Jülich,
521 ISBN ISBN 978-3-95806-619-9 (2022).